Joseph G. Craig
Lily Go
Joseph Blechinger
David Hearshen
J. Antonio Bouffard
Mark Diamond
Marnix T. van Holsbeeck

Three-tesla imaging of the knee: initial experience

J. G. Craig (✉) · J. Blechinger ·
D. Hearshen · J. A. Bouffard ·
M. Diamond · M. T. van Holsbeeck
Department of Diagnostic Radiology,
Henry Ford Hospital,
2799 West Grand Boulevard,
Detroit, MI, 48202, USA
e-mail: josephc@rad.hfh.edu
Fax: +1-313-9169475

L. Go
Wayne State University
School of Medicine,
Detroit, MI, USA

Abstract *Purpose:* To assess 3-T imaging of the knee. *Materials and methods:* We reviewed 357 3-T magnetic resonance images of the knee obtained using a dedicated knee coil. From 58 patients who had arthroscopy we determined the sensitivity and specificity for anterior cruciate ligament (ACL) tear and medial and lateral meniscal tear. *Results:* A chemical shift artifact showed prominently at 3 T even after improvements had been made by increasing the bandwidth. For complete ACL tear the sensitivity was 100% (95% confidence interval, CI, 75.30–100.00), and the specificity was 97.9% (95% CI 87.7–99.9). For the medial meniscus the sensitivity was 100.00% (95% CI 90.0–100.00), and the specificity was 83.3%(95% CI 66.6–95.3). For the lateral meniscus the sensitivity was 66.7% (95% CI 38.4–88.2), and the specificity was 97.6% (95% CI 87.1–99.9). *Conclusions:* In general 3-T imaging allows a favorable display of anatomy and pathology. The lateral meniscus was assessed to be weaker than the other anatomic structures. Three-tesla imaging allows increased signal-to-noise ratio, increased resolution, and faster scanning times.

Keywords Knee, MR · Knee, ligament, menisci and cartilage · MR, high-field-strength imaging

Introduction

Magnetic resonance (MR) is of proven value in assessment of the knee. Tears of the anterior cruciate ligament and menisci can be assessed with high accuracy [1–15]. High-field-strength 3-T imaging allows increased signal-to-noise ratio (SNR), increased resolution, and faster imaging. Clinical 3-T imaging has only recently become available for routine clinical use. In this paper, we present our initial experience with 3-T imaging of the knee.

Materials and methods

With the approval of our Institutional Review Board we reviewed the knees of 343 patients (177 male, 166 female, age range 12–88 years) who had an MR examination of the knee with a 3-T magnet. Fourteen patients had bilateral knee examinations to give a total of 357 consecutive knees (183 right knees, 174 left knees). The scans were carried out with a dedicated 3-T Signa Clinical Magnet (GE Medical Systems, Milwaukee, WI, USA). We modified our regular 1.5-T knee protocol for 3-T imaging. The 3-T regular knee protocol consists of sagittal and coronal proton-density-weighted fast spin echo sequences (echo train 7–8, repetition time, TR, 3,000–4,000 ms, echo time, TE, 11–12 ms, bandwidth 62.5 kHz, 512×256 acquisition matrix, 3-mm/1-mm interspace, one signal average), and axial and coronal fast spin echo fat-suppressed T2-weighted sequences (echo train 10–12, TR 3,000–4,000 ms, TE 80–90 ms, bandwidth 31.25 kHz, 352×192 matrix for the axials, 384×192 for the coronals, 4-mm/1-mm interspace with two signal averages). To obtain our final 3-T protocol progressive adjustments were made to the 1.5-T protocol. Ini-

tially 22 coronal proton density examinations were acquired with a 320×256 matrix, and one with a 256×192 matrix. Six sagittal proton density series were acquired with a 512×192 matrix, and one with a 256×192 matrix. Two coronal proton density sequences were acquired with a TR of 2,000–3,000 ms. Thirty-four coronal proton density sequences were acquired with a TR of 4,000–5,000 ms, the majority just above 4,000 ms. One coronal proton-density sequence had a TR of 6,517 ms. Thirty-two sagittal proton density sequences were acquired with a TR of 2,000–3,000 ms, all but one of these having a TR of 2,500–3,000 ms. Four sagittal proton density sequences had a TR of 4,000–5,000 ms. For the axial T2 sequences 14 were acquired with a TR of 2,500–3,000 ms, the majority just below 3,000 ms. Three axial T2 sequences had a TR just above 4000 ms, a fourth had a TR of 4,800 ms and a fifth had a TR of 5,550 ms. Fifty-seven coronal T2 sequences were acquired with a TR of 5,000–6,500 ms. Two further se-

quences had TRs of 6,600 and 6,950 ms, respectively. Of the T2 sequences 18 had and an echo train of 6–9, and 127 an echo train of 13–16. In the majority of knees (287) the proton density series were reconstructed with a 1,024× 1,024 matrix. The field of view was 14–18 cm. All of the knee examinations were obtained using a dedicated GE Medical Systems Quadrature extremity knee coil. The total scanning time was in the order of 10–12 min. The MR examinations were read by one of four experienced musculoskeletal radiologists.

Fifty-eight patients were present in the arthroscopy group (39 male, 19 female, 24 right knees, 34 left knees, age range 13–68 years.) For these 58 patients we reviewed the original radiological report and the operative note and
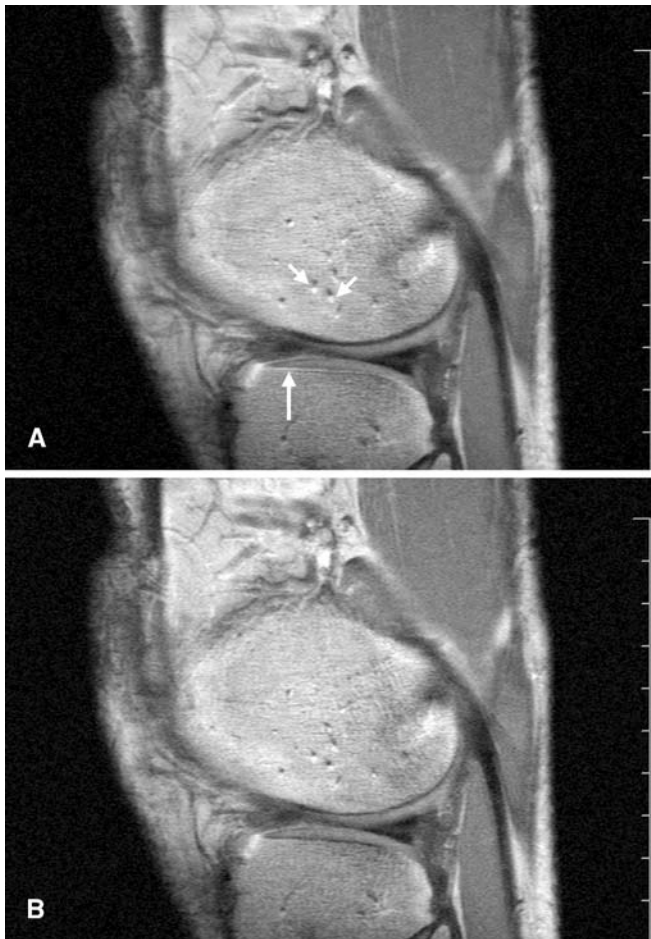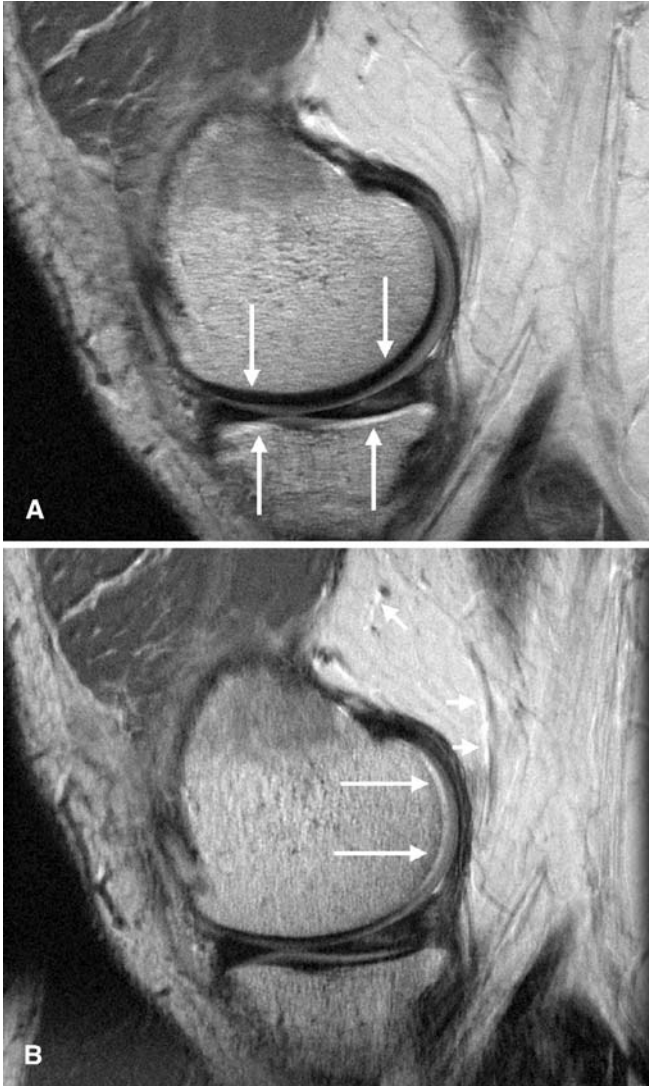

Fig. 1A, B Chemical shift artifact. **A** Sagittal proton density image (31.25kHz, 3,000/15 eff, echo train 8) shows a chemical shift artifact adjacent to the subchondral bone plate (*long arrows*) and the vessels in the femoral condyle (*short arrows*). **B** Sagittal proton density image at higher bandwidth (62.5 kHz, 3000/12 eff, echo train 8) still shows the chemical shift artifact but it is less prominent than in **A**
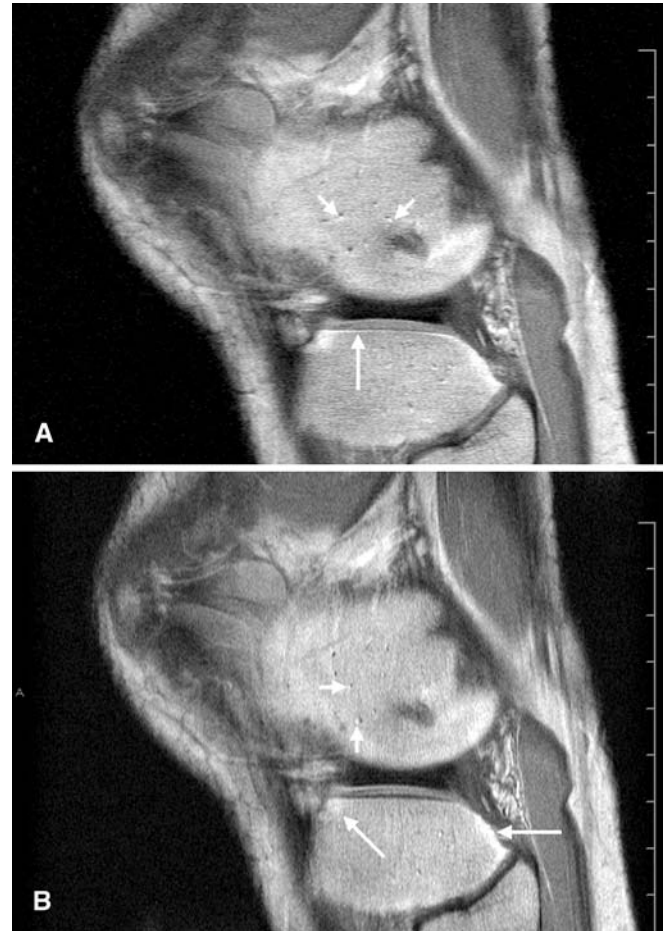

Fig. 2A, B Chemical shift artifact. **A** Sagittal proton density image (62.5 kHz, 3,000/12 eff, echo train 8) shows a chemical shift artifact adjacent to the subchondral bone plate (*long arrow*) and the vessels in the femoral condyle (*short arrows*). **B** Sagittal proton density image (62.5 kHz, 3,000/12 eff, echo train 8) shows that when the frequency is changed 90° the chemical shift artifact disappears from the subchondral bone and the artifact adjacent to the vessels moves 90° clockwise (*short arrows*). The residual increased signal at the margins of the tibial cortex (*long arrows*) is more difficult to explain and may represent a chemical shift artifact in the slice-selection direction

then determined the sensitivity and specificity for full-thickness anterior cruciate ligament (ACL) tear and for meniscal tear. Two ACLs had been reconstructed and were therefore excluded from the statistical analysis. One ACL was read preoperatively as "intrasubstance degeneration/tear," and another as "sprain of the ACL." Both of these were included in the negative group for full-thickness tear. Three medial menisci were read preoperatively as "menisco-capsular separation." These results were interpreted as meaning a peripheral tear in the vascularized portion of the medial meniscus and were included in the group

positive for meniscal tear. Two lateral menisci had been partially resected and were excluded from the analysis. One lateral meniscus was read as "frayed" preoperatively and two lateral menisci were described as "frayed" intraoperatively. These were placed in the preoperative and postoperative groups negative for meniscal tear. Fifty-six of the

Fig. 3A, B Chemical shift artifact. **A** Sagittal proton density image (15.6 kHz, 4,000/24 eff, echo train 8) shows a chemical shift artifact with widening of the subchondral bone plate of the femur and thinning of the plate of the tibia (*arrows*). **B** With the frequency changed 90° the sagittal proton density image (15.6 kHz, 4,000/24 eff, echo train 8) shows the subchondral bone plate of the femur is now thinned posteriorly (*long arrows*). Note also the chemical shift artifact adjacent to the vessels in the posterior femoral fat has moved 90° (*short arrows*)
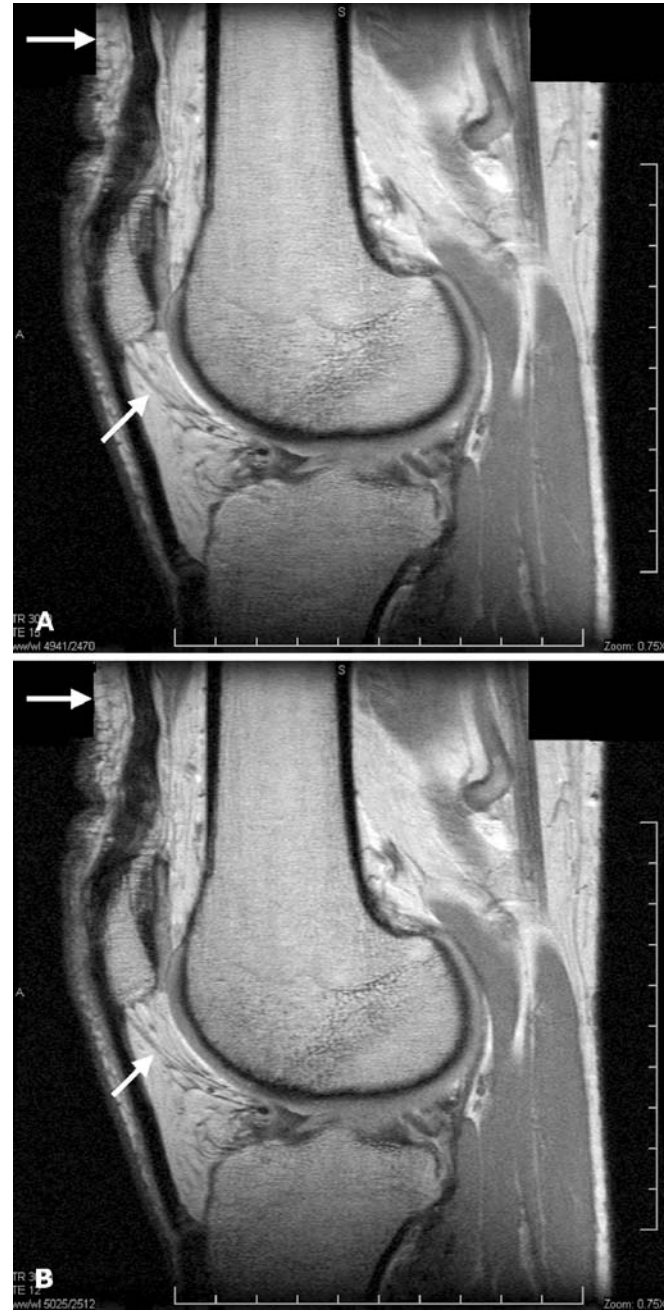
Fig. 4A, B Fast spin echo blurring versus bandwidth. **A** On the sagittal proton density image (31.25 kHz, 3,000/15 eff, echo train 8) note the blurring of the stranding in Hoffa's fat pad and in the anterior subcutaneous fat (*arrows*). **B** At higher bandwidth, the sagittal proton density image (62.5 kHz, 3,000/12 eff, echo train 8) shows the stranding to be sharper (*arrows*)

arthroscopies were performed by one of five orthopedic surgeons, four of whom were from our Sports Medicine Department. One of two other orthopedic surgeons performed the other two arthroscopies respectively. The time from MRI to arthroscopy varied from 3 to 106 days with an average of 56 days.
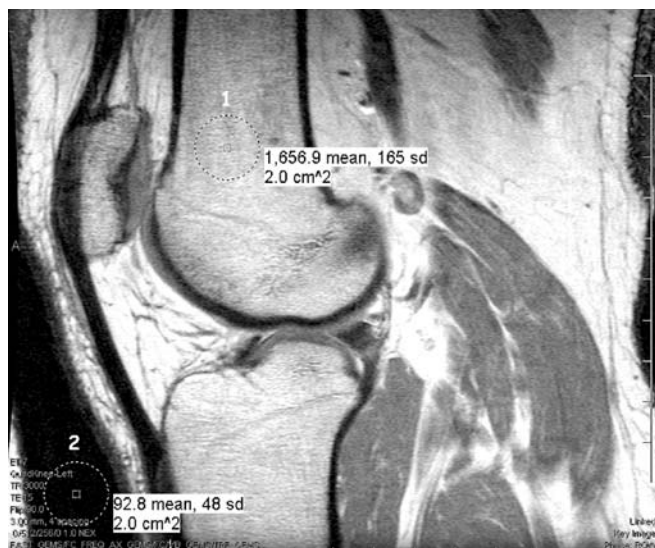
We determined the SNR when using the higher 62.5-kHz bandwidth. The SNR was determined by measurement of the average signal in a 2.0-cm^2 region of the distal femur and the standard deviation of the noise from air. Identical areas at the 31.25- and 62.5-kHz bandwidths were measured to make this determination.

We initially altered the bandwidth between 31.25 and 62.5 kHz on the proton density images and also altered the frequency direction in a small subgroup of patients to determine the best protocol for the proton-density images.

For one volunteer we altered the bandwidth between 62.5, 31.25 and 15.6 kHz on the proton density images using a 512×512 matrix to assess the subchondral bone plate chemical shift artifact. For the 15.6-kHz series we also changed the frequency 90° and assessed the effect on image quality.

Results

Three-tesla imaging allowed increased SNR, faster imaging, and increased resolution. A chemical shift artifact was more noticeable at 3 T with both the 31.25- and the 62.5-

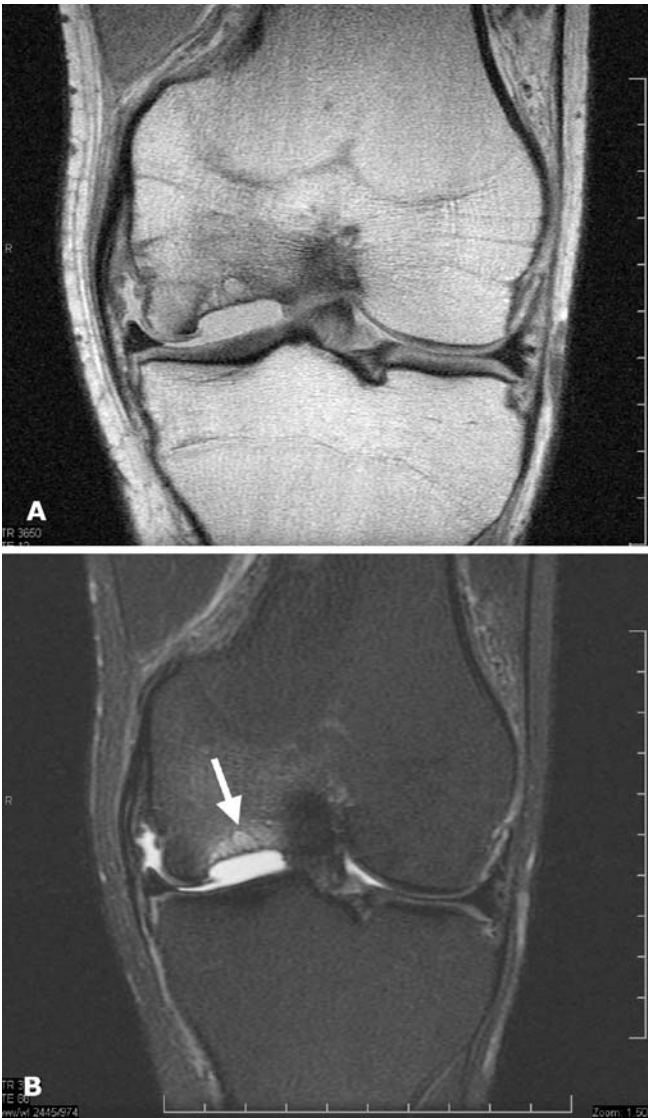kHz bandwidths although it was less with the higher bandwidth (Figs. 1, 2, 3).

Use of the higher 62.5-kHz bandwidth resulted in less blurring of the fast proton density images (Fig. 4).

The SNR of the muscle when scanned with a receive bandwidth of ±31.25 kHz was 34.5 and with a bandwidth of ±62.5 kHz it was 28.2 (Fig. 5). The change was 18.3%. The minimum effective TE changed with the bandwidth from 15 to 12 ms at 32.25 and 62.5 kHz, respectively.

There was excellent visualization of hyaline cartilage on the fast proton density images (Figs. 6, 7).
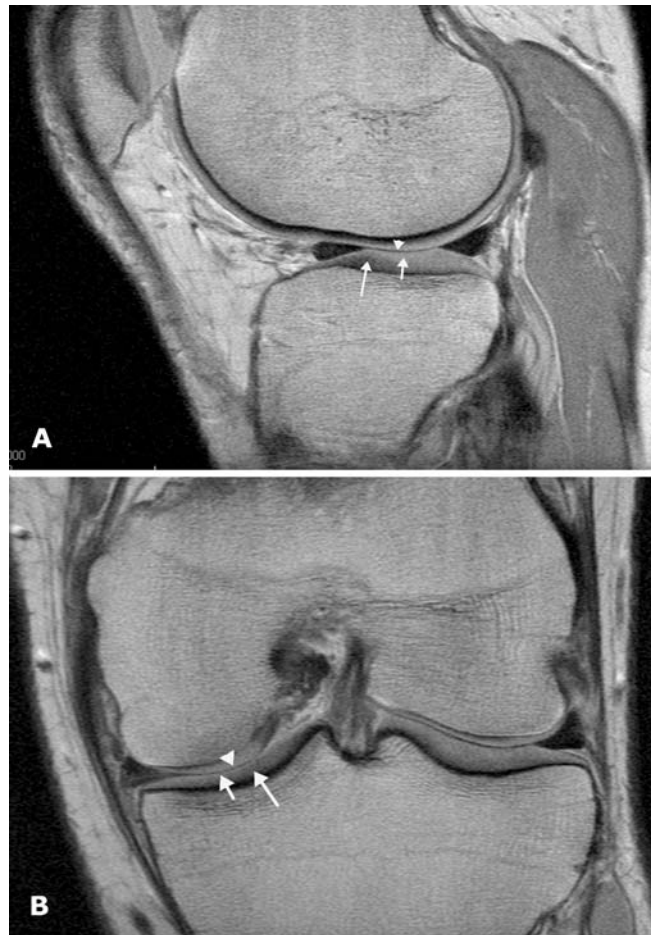
Fig. 6A, B Normal cartilage on fast proton density images. **A** Sagittal fast proton density image (3,000/12 eff, echo train 8, 512×256, 62.5 kHz, 14-cm field of view, *FOV*) shows excellent definition of hyaline cartilage. Note the changes in the tibial hyaline cartilage. A low-signal-intensity deep layer is present with vertical striations (*long arrow*). Above this is a higher-signal-intensity transitional layer (*short arrow*) and a thin low-signal-intensity superficial layer (*arrowhead*). Note also the thickness of this stratification varies across the tibial cartilage. **B** Coronal fast proton density image (3,000/12, echo train 8, 512×256, 62.5 kHz, 14-cm FOV) also shows an excellent definition of cartilage. Note again the changes in the tibial hyaline cartilage (*arrows*, *arrowhead*) and observe that the thickness of the layers varies across the tibial cartilage

Fig. 5 Signal-to-noise ratio (*SNR*) at 31.25 and 62.5 kHz. The SNR was estimated from the signal in the distal femur, region *1* and the noise as the standard deviation in the air anterior to the knee, region *2*. The same slice of the same subject and identical positions were used for the SNR comparisons at 62.5 and 31.25 kHz. The doubling of the bandwidth should lead to a 42% decrease in SNR. However the effective echo time decreases with bandwidth change, which increases the signal. The net result is the SNR decreased by 18.3% at the higher bandwidth

Fig. 7A, B Osteochondral injury. **A** Coronal fast proton density image (3,650/12 eff, echo train 8, 62.5 kHz, 512×256, 14-cm FOV) clearly demonstrates the large osteochondral defect in the weight-bearing portion of the medial femoral condyle. Note also the excellent definition between hyaline cartilage and fluid. **B** Coronal fast fat-suppressed T2-weighted image (3,767/88 eff, 384×192, echo train 10) clearly shows the defect with adjacent edema in the medial femoral condyle (*arrow*)

Of the ACLs 13 complete ruptures were accurately diagnosed (Fig. 8). One false-positive diagnosis of chronic tear of the ACL was made (Fig. 9). For the medial meniscus 34 meniscal tears were accurately diagnosed (Fig. 10). There were four false-positive diagnoses of medial meniscal tear (Fig. 11). For the lateral meniscus ten lateral meniscal tears were accurately diagnosed (Fig. 12). There was one false-positive diagnosis of lateral meniscal tear and five false-negative diagnoses (Figs. 13, 14).

Our results for the ACL and the medial and lateral menisci are summarized in Table 1.

Fig. 8 Anterior cruciate ligament (*ACL*) tear, true positive. Sagittal proton density image (3,000/12 eff, echo train 8) through the intercondylar notch shows a large hematoma secondary to an acute ACL tear (*arrows*)

Discussion

A 3-T magnetic field offers an increase in SNR. This increase can be utilized to improve image quality by offering options to increase resolution or decrease scan time and the chance for motion artifacts. Clinical 3-T imaging has only recently become available and allows an excellent display of both anatomy and pathology and is capable of producing imaging superior to that at 1.5 T. We were able to move

Fig. 9 ACL tear, false positive. Sagittal proton density image (3,000/12 eff, echo train 8) shows ill definition of the ACL near its tibial attachment (*arrows*). This was diagnosed as "degeneration and chronic tear." At arthroscopy, the ACL was intact
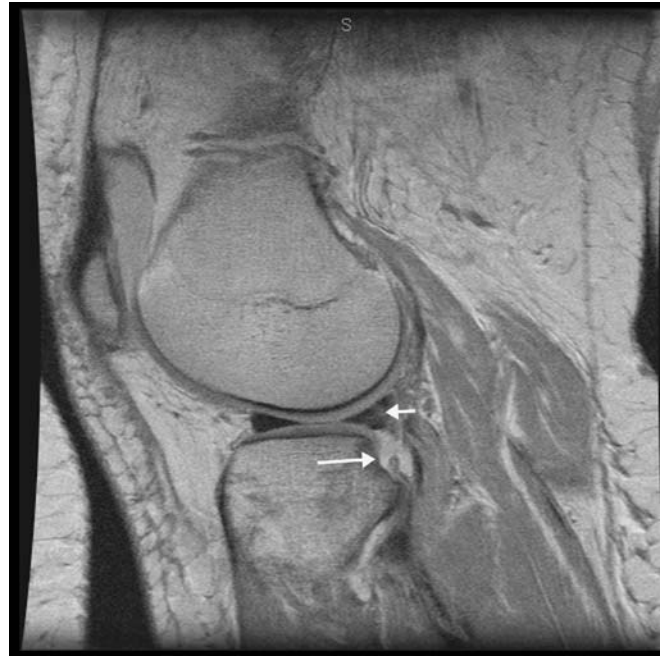
Fig. 10 Medial meniscal tear, true positive. Coronal fast proton density image (3,000/12 eff, echo train 8) shows a bucket handle tear involving the medial meniscus (*arrows*). There was also a complete tear of the ACL

to 3-T imaging of the knee with only minor modifications of our original 1.5-T protocols. We noted in general a favorable display of anatomy and pathology with good intrinsic contrast between fat, muscle, fluid, fibro-cartilage, and hyaline cartilage. In particular, very good definition of hyaline cartilage on fast proton density images was observed (Figs. 6, 7).

Fig. 11 Medial meniscal tear, false positive. Sagittal fast proton density image (3,616/12 eff, echo train 8) shows a linear signal consistent with a tear at the junction of the vascularized and nonvascularized portions of the meniscus (*arrow*). The change was interpreted preoperatively as a menisculo-capsular separation. At arthroscopy, the meniscus appeared intact. There was also an acute ACL tear

Fig. 12 Lateral meniscal tear, true positive. Sagittal fast proton density (3,217/12 eff, echo train 8) shows a complex tear of the lateral meniscus (*short arrow*). Note also the impaction fracture of the posterior tibial plateau (*long arrow*). There was an associated ACL tear

In clinical practice a chemical shift artifact is certainly more noticeable at 3 T when compared with 1.5 T (Figs. 1, 2, 3, 4). The doubling of the separation between the resonant frequencies between fat and water leads to improved fat saturation but also introduces a chemical shift artifact. The artifact is apparent in the image as a spatial shift of fat in the frequency-encoded direction. When first tested at 3 T, our 1.5-T protocol had an artifact because of the fat shift. After increasing the scan resolution to 512 from 256 the artifact became significant, moving four pixels. To compensate for the chemical shift artifact, we increased the bandwidth from 31.25 to 62.50 kHz. Even with the higher bandwidth, the artifact is still seen, although it is not as distracting. With both bandwidths, we did not see any cases in which a chemical shift artifact obscured relevant diagnostic information. A subchondral bone plate chemical shift artifact is certainly very prominent at 15.6 kHz (Fig. 3); however, no clinical cases were investigated using this bandwidth. At 62.5 kHz, although still present it is less noticeable and we did not have any cases in which it affected our overall interpretation. It was difficult to explain the anatomic basis of some of the chemical shift artifact (Fig. 2). Some of this artifact may be from a chemical shift not in the frequency direction, but in the slice direction [16].

An advantage of increasing the bandwidth when using fast spin echo sequences is that the blurring of the image is less (Fig. 3). A major disadvantage, however, is that the

Fig. 13 Lateral meniscal tear, false positive. Sagittal fast proton density image through the lateral femoral condyle (3,000/12 eff, echo train 8) shows an irregular anterior horn with signal going to the tibial surface (*short arrow*), called a "complex tear." At arthroscopy, the meniscus was noted to be "frayed but intact." Some of the changes around the anterior horn may relate to scarring from the prior arthroscopy portal used for an ACL reconstruction (*long arrows*)

Fig. 14 Lateral meniscal tear, false negative. Sagittal fast proton density image through the lateral femoral condyle (3,200/12 eff, echo train 8) shows an unremarkable lateral meniscus. At arthroscopy, a small radial tear between the anterior and the middle thirds was noted. There was an associated ACL tear

SNR decreases. Clinically, there was no obvious decrease in the SNR when comparing the lower and higher bandwidth images and the higher bandwidth images appear sharper owing to less blurring (Fig. 4). The reduction in the SNR due to the increase in bandwidth tracks as the square root of the change. The doubling of the bandwidth should lead to a 41% decrease in the SNR; however, the effective TE decreases with the bandwidth change, which increases the signal. The net result is the SNR decreased by only 18.3% (Fig. 5).

On fast spin echo proton density weighted images, we found that there was excellent definition of both normal and abnormal hyaline cartilage. Of particular note, changes of the extracellular cartilage matrix were clearly visualized (Fig. 6). The appearance of hyaline cartilage on MRI has previously been documented, most recently by Goodwin et al. [17–19]. Variation in the T2 signal decay across hyaline cartilage produces a layered appearance [19]. Tibial cartilage displays a thin, low-signal-intensity surface layer, a higher-signal-intensity transition layer and a low-signal-intensity deep layer in which vertical striations are present. The relative thicknesses of these layers also differ. In the central region of the tibial plateau the thick, deep layer extends across the cartilage, whereas at the joint periph-ery transitional and surface layers are larger [19]. These changes reflect the structure of the extracellular matrix and are clearly visualized on proton density images at 3 T (Fig. 6).

Diagnosis of complete tear of the ACL was satisfactory with one false positive. The interpretation of the single false-positive case may have been influenced by an apparent full-thickness tear of the ACL in that knee on MRI 3 years earlier. Diagnosis of medial meniscal tear was also satisfactory with 34 true positives and four false positives. Three of the four false-positive diagnoses were associated with ACL tear and the changes seen on MRI were in the vascularized portion of the meniscus or at the junction of the vascularized and nonvascularized portions of the meniscus (Fig. 11). In these cases it is possible that the changes were too peripheral for the arthroscopist to visualize, or that the tear had healed prior to arthroscopy. In the fourth case with retrospective analysis the signal went to the tibial surface on only one section and could be considered equivocal for tear.

The sensitivity result for the lateral meniscus was disappointing. Five lateral meniscal tears were missed. It has been noted that associated ACL tear decreases the sensitivity for lateral meniscal tear [8], although only two of the missed tears were associated with this. With retrospective analysis three of the five tears could still not be seen; one was marginal at best; in the fifth case the tear could be visualized but the meniscus was called "frayed" rather than

Table 1 Results for the anterior cruciate ligament, the medial meniscus, and the lateral meniscus

		Estimate	95% confidence interval
Anterior cruciate ligament	Sensitivity	100.0 (13/13)	75.3–100.0
	Specificity	97.7 (42/43)	87.7–99.9
	Predictive value positive	92.9 (13/14)	66.1–99.8
	Predictive value negative	100.0 (42/42)	91.6–100.0
Medial meniscus	Sensitivity	100.0 (35/35)	90.0–100.0
	Specificity	83.3 (20/24)	62.6–95.3
	Predictive value positive	89.5 (34/38)	75.2–97.1
	Predictive value negative	100.0 (20/20)	83.2–100.0
Lateral meniscus	Sensitivity	66.7 (10/15)	38.4–88.2
	Specificity	97.6 (40/41)	87.1–99.9
	Predictive value positive	90.9 (10/11)	58.7–99.8
	Predictive value negative	88.9 (40/45)	75.9–96.3

p values*

Comparison	Sensitivity	Specificity	Predictive value positive	Predictive value negative
All vs. medial meniscus	0.9999	0.0517	0.9999	0.9999
All vs. lateral meniscus	0.0437	0.9999	0.9999	0.0561
Medial meniscus vs. lateral meniscus	**0.0016**	0.0579	0.9999	0.3128

*To be significant the *p* values in order (smallest to largest) must be less than 0.0167, 0.0250, and 0.0500, respectively.

torn. Our arthroscopy numbers are not large, and in particular the numbers for lateral meniscal tear are small as reflected in the wide CIs in the statistical analysis. Whether the low sensitivity reflects problems with interpretation of the tear at the original reading, a particular problem with 3-T imaging for the lateral meniscus, or simply the small numbers cannot be stated with certainty. However, the latter possibility seems most likely.

Limitations of this study include the fact that the imaging parameters were not standardized and hence it is difficult to make a categorical analysis of the results. The very disappointing results for lateral meniscal tear are also a problem although, as discussed earlier, the arthroscopy numbers are not large and there are wide CIs in the statistical analysis. A prospective study with standardized technical parameters would better address this last point. With the increased number of 3-T scanners used for clinical imaging, primarily at present for neuroradiology im-

aging, there will be further musculoskeletal applications including the knee, but further research is needed to investigate and document advantages of the higher field strength.

In summary, we reviewed 357 3-T images of knees, with 58 patients having arthroscopy. Very good intrinsic contrast was noted between fat, muscle, hyaline cartilage, fibrocartilage, and fluid. We were able to produce excellent images with fast scanning times (the total examination scanning time was 10–12 min, more recently with an upgrade to 8.5–9 min). Diagnosis of ACL tear and medial meniscal tear was satisfactory, but the sensitivity for lateral meniscal tear was disappointing, although our numbers are small. With very little motion and good intrinsic contrast between fat, muscle, fluid, hyaline, and fibro-cartilage the musculoskeletal system seems ideally suited to 3-T imaging and certainly there will be further applications.

References

1. Chan WP, Peterfy C, Fritz RC, Genant HK. MR diagnosis of complete tears of the anterior cruciate ligament of the knee: importance of anterior subluxation of the tibia. AJR Am J Roentgenol 1994; 162:355–360.
2. McCauley TR, Moses M, Kier R, Lynch JK, Barton JW, Jokl P. MR diagnosis of tears of anterior cruciate ligament of the knee: importance of ancillary findings. AJR Am J Roentgenol 1994; 162:115–119.
3. Murphy BJ, Smith RL, Uribe JW, Janecki CJ, Hechtman KS, Mangasarian RA. Bone signal abnormalities in the posterolateral tibia and lateral femoral condyle in complete tears of the anterior cruciate ligament: a specific sign? Radiology 1992; 182:221–224.
4. Tung GA, Davis LM, Wiggins ME, Fadale PD. Tears of the anterior cruciate ligament: primary and secondary signs at MR imaging. Radiology 1993; 188:661–667.
5. Vahey TN, Hunt JE, Shelbourne KD. Anterior translation of the tibia at MR imaging: a secondary sign of anterior cruciate ligament tear. Radiology 1993; 187:817–819.
6. Remer EM, Fitzgerald SW, Friedman H, Rogers LF, Hendrix RW. Anterior cruciate ligament injury: MR imaging diagnosis and patterns of injury. Radiographics 1992; 12:901–915.
7. Crues JV 3rd, Mink J, Levy TL, Lotysh M, Stoller DW. Meniscal tears of the knee: accuracy of MR imaging. Radiology 1987; 164:445–448.
8. De Smet AA, Graf BK. Meniscal tears missed on MR imaging: relationship to meniscal tear patterns and anterior cruciate ligament tears. AJR Am J Roentgenol 1994; 162:905–911.
9. Mink JH, Levy T, Crues JV 3rd. Tears of the anterior cruciate ligament and menisci of the knee: MR imaging evaluation. Radiology 1988; 167:769–774.
10. Boeree NR, Watkinson AF, Ackroyd CE, Johnson C. Magnetic resonance imaging of meniscal and cruciate injuries of the knee. J Bone Joint Surg Br 1991; 73:452–457.
11. Mackenzie R, Palmer CR, Lomas DJ, Dixon AK. Magnetic resonance imaging of the knee: diagnostic performance studies. Clin Radiol 1996; 51:251–257.
12. Rubin DA, Paletta GA Jr. Current concepts and controversies in meniscal imaging. Magn Reson Imaging Clin North Am 2000; 8:243–270.
13. Escobedo EM, Hunter JC, Zink-Brody GC, Wilson AJ, Harrison SD, Fisher DJ. Usefulness of turbo spin-echo MR imaging in the evaluation of meniscal tears: comparison with a conventional spin-echo sequence. AJR Am J Roentgenol 1996; 167:1223–1227.
14. Cheung LP, Li KC, Hollett MD, Bergman AG, Herfkens RJ. Meniscal tears of the knee: accuracy of detection with fast spin-echo MR imaging and arthroscopic correlation in 293 patients. Radiology 1997; 203:508–512.
15. Rubin DA, Kneeland JB, Listerud J, Underberg-Davis SJ, Dalinka MK. MR diagnosis of meniscal tears of the knee: value of fast spin-echo vs. conventional spin-echo pulse sequences. AJR Am J Roentgenol 1994; 162:1131–1135.
16. Hendrick RE, Russ PD, Simon JH. MRI: principles and artifacts. New York: Raven; 1993: 191–192.
17. Mlynarik V, Degrassi A, Toffanin R, Vittur F, Cova M, Pozzi-Mucelli RS. Investigation of laminar appearance of articular cartilage by means of magnetic resonance microscopy. Magn Reson Imaging 1996; 14:435–442.
18. Xia Y, Farquhar T, Burton-Wurster N, Lust G. Origin of cartilage laminae in MRI. J Magn Reson Imaging 1997; 7:887–894.
19. Goodwin DW, Wadghiri YZ, Zhu H, Vinton CJ, Smith ED, Dunn JF. Macroscopic structure of articular cartilage of the tibial plateau: influence of a characteristic matrix architecture on MRI appearance. AJR Am J Roentgenol 2004; 182:311–318.